The pulse-pile-up tail artifact in pulse-height spectra

T. Ahsan,[1,2] C.P.S. Swanson,[2,3] T. Qian,[2] T. Rubin,[2] and S.A. Cohen[2]
[1)]*Physics Department, Princeton University, Princeton, NJ, 08540 USA*
[2)]*Princeton Plasma Physics Laboratory, Princeton University, Princeton, NJ, 08543 USA*
[3)]*Princeton Fusion Systems, Plainsboro, NJ,08536 USA*

(*Electronic mail: scohen@pppl.gov)

(Dated: 19 July 2021)

Pulse pile-up in pulse-height energy analyzers increases when the incident rate of pulses is comparable to or larger than the pulse pair resolving time of the detection system. Large changes in the observed energy distributions with incident rate and pulse shape then occur. In this paper we focus on the high energy tail of X-ray spectra, important for measurements on partially ionized, warm, pure-hydrogen plasma. A two-photon pulse-pile-up model is derived for trapezoidal-shaped pulses produced in Amptek Fast SDD detectors and quantitative agreement is found between the measurements and the model predictions.

I. INTRODUCTION

Solid-state detectors operating in the pulse-height mode are used to measure energy distributions of incident radiation.[1,2] In these detectors, the amount of electrical charge released by the impact of a single photon, is proportional to the energy of the photon. The energy resolution of these detectors is set by the timing and statistics of the generated and integrated charge, thermal noise, and the accuracy of the conversion of that charge to voltage.[3] In this paper, we will discuss X-ray photon detection only although the method can be applied to charged particles.

Pulse-height X-ray detectors are used for applications where moderate resolution over a broad energy spectrum is more advantageous than high resolution in a narrow spectrum. The latter, for example, is obtainable with a crystal spectrometer.[4] The former is preferred for applications such as X-ray fluorescence spectroscopy of material samples[5] and electron temperature measurement *via* broad-spectrum Bremsstrahlung in warm or hot plasmas.[6]

Our experiments explore nearly pure, > 99 %, partially ionized, warm hydrogen plasmas. For these, interest lies in the tails of the X-ray spectrum, not in peaks often used to identify and quantify elemental composition. In plasmas, small tails of high-energy electrons in the energy distribution, even comprising less than 0.1% of the plasma density, can have large effects on plasma resistivity, stability, and reaction rates. Thus, this paper reports on a topic usually not encountered in the elemental-analysis application of silicon drift detectors (SDDs), but in an arena extending their use.

Because the free charge generated in SDDs is approximately 4.4×10^{-20} C/eV of incident photon energy,[7] the useful low energy limit of these detectors, based on resolution, is about 100 eV. These detectors are sensitive to lower-energy photons (VUV, UV, and visible), though only at high fluxes and not spectrally resolved.[5]

For a large photon flux, more than one may arrive at the detector within the time that the free charge is integrated into a voltage signal, the pulse pair resolving time, or PPR time t_p. It is the minimum time between two pulses at which they can be recognized by the electronics as two distinct pulses. As a result, the detector interprets near-coincident impacts of multiple photons as a single photon with energy equal to the sum of the energies from the multiple impacts. This is called pulse pile-up (PPU).

PPU can be strongly mitigated in most circumstances using pile-up rejection (PUR) which can be accomplished in several ways. For example, in the Amptek X-123 Fast SDD, whose typical operational parameter are listed in Appendix 1, the energy of a pulse is determined using a slow channel which typically filters by a microsecond, while the timing of a pulse is determined using a fast channel, typically filtering by tens of nanoseconds. If the fast channel measures two pulses within a PPR time of the slow channel, both pulses are rejected.[5]

There are circumstances in which PUR is ineffective, such as when the X-ray spectrum is quasi-Maxwellian. Then the tail inferred for the spectrum may be compromised by a much brighter low energy part of the true spectrum. Several low-energy photons may arrive within the 10‘s of ns of the fast channel's PPR time. (This contrasts with a common use of pulse-height energy detectors that concentrates on peaks whose heights are well above a relatively low background.)

For example, X-ray emission from the PFRC-2 plasma experiment[8] often shows an emitted X-ray spectrum arising from a Maxwellian distribution of electrons with density $n_e \sim 1 \times 10^{12}$ /cm^3 and temperature $T_e \sim 100$ eV. Additionally, the spectrum shows a large flux of lower energy photons, attributable to VUV.

Amptek SDDs are available with a variety of windows. Some are Be ones of selectable thickness; others are thin Si_3N_4 structures and named C1 and C2. C-series windows allow observation to below 200 eV. We use a C1 window, which is not completely opaque to VUV photons, having a transmissivity to 73 eV photons as high as 14%.[9]

Three PFRC-2 X-ray spectra are shown in Figure 1, all obtained with the PFRC-2's central magnetic field at 220 G, a hydrogen pressure in the central cell of 0.39 mTorr, an RMF frequency of 6.05 MHz, an RMF forward power of 52 kW, and a discharge duration of 4.7 ms. (RMF is the name of the RF heating technique.) X-rays were accumulated from about 1000 discharges. The higher CR was achieved by increasing an aperture's size in a stainless steel shield in front of the SDD.

The slope of the spectrum changes above 100 eV, becom-

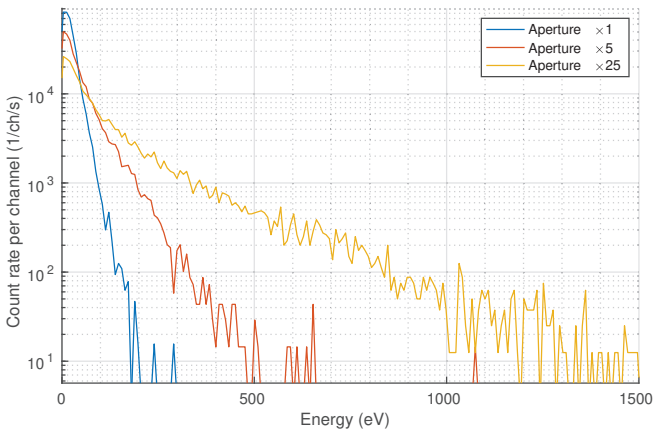

FIG. 1. PFRC-2 X-ray spectra *vs* aperture area for the same plasma parameters. The relative aperture areas are noted in the legend. PUR was not enabled for these measurements.

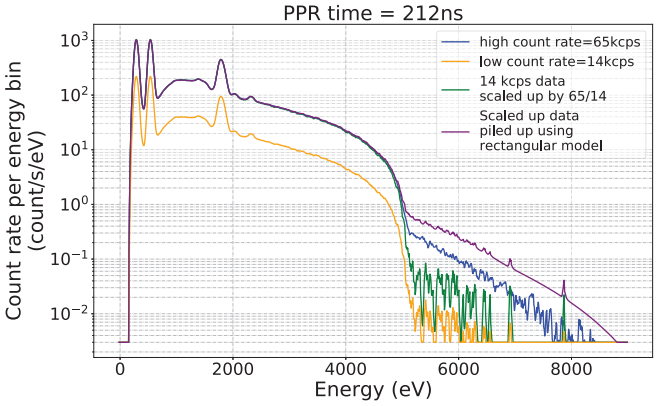

FIG. 2. X-ray spectra (14 kcps and 65 kcps) for a 5-keV electron beam impacting a carbon target and predicted spectra using the rectangular model[12]. Noise was reduced using a $\sim$ 50-eV-wide weighted moving average filter. The slow-channel PPR time was 212 ns.

ing shallower with a greater count rate (CR), incorrectly attributable to photons with apparent energy above 100 eV. Concurrent with the increase in slope is a decrease in the spectrum amplitude at 50 eV, another indicator of PPU.[6,10,11] Activating PUR proves ineffective at eliminating this piled-up spectrum, as the fast channel and slow channel average over UV flux using different timescales. This piled-up spectrum obscures the true soft X-ray spectrum. We would like to characterize this pulse pileup, so that we can asses measures to eliminate this pileup and measure the true soft X-ray spectrum.

To study this immitigable PPU and test models, we have measured X-ray emission from a graphite-target X-ray tube with incident electron energy $E_e = 5$ keV. Using a solid graphite target reducess poorly quantifiable VUV emission – estimated to be due atomic hydrogen lines in the PFRC-2 experiments – that generates the PPU. This allows quantitative measurement of PPU. For these measurements, we disabled the SDD's PUR features. Figure 2 shows spectra measured using high and low X-ray tube electron currents, corresponding to higher and lower X-ray CRs. At low count rate, 14 kcps (yellow), the spectrum has visible spectral lines and solid-target Bremsstrahlung. The ratio of the 1740 eV Si peak to the signal at 5 keV is 10^4. At higher count rate, 65 kcps (green), the ratio has dropped to 1,300, indicating PPU. The PPU-generated tail above 5 keV has a near-exponential shape. The target current was 190 nA for 14 kcps and 750 nA for 65 kcps and target voltage was 5 keV for both. The dead time for 14 kcps data is 0.5% and 2.3% for the 65 kcps data .

As a result of PPU, the measured energy spectrum is corrupted in two ways. First, PPU adds a tail to the distribution, which, in the case of 2-photon pile-up, could reach up to twice the maximal photon energy in the experiment. This paper uses this feature of the PPU effect to validate the proposed pile-up model. Second, PPU may produce false peaks in the distribution, located at the sum of the energies of two peaks. Even though the physics of the two PPU effects is the same, the data interpretation might be different. Peaks in the distribution may correspond to elemental line radiation in an X-ray tube target, gamma radiation of radionuclides, or several other photon scattering mechanisms, *e.g.*, Compton scattering. As noted earlier, this paper restricts attention to tails in spectra.

The effect of PPU has been previously discussed by many authors. Datlowe analyzed the role of the shape of the waveform in PPU and developed a method to calculate the effects efficiently.[13] Guo, *et al*. used a Monte-Carlo method MCPUT to correct the spectral distortion from PPU.[14] Taguchi, *et al.* derived and used methods to correct the peak and tail pile-up effect for non-paralyzable detectors.[15] Wang, *et al.* analyzed the effect of pulse pile-up on the spectrum for a double-sided silicon strip detector for different pulse shapes, accounting for the spatial distribution of photon interactions.[16] However, the effect of trapezoidal pulse shape, a technique used in many pulse-height detection systems, on the measured energy distribution function has not previously been analyzed in detail.

Amptek X-123 Fast SDD pulse-height X-ray systems[6,12,17] were used to detect and analyze X-rays emitted by electrons in PFRC-2 plasma; we have discussed the interpretation of that data[6] without including PPU analyses and with the key objective to extract the electron energy distribution function (EEDF) from the X-ray energy distribution function (XEDF). The X-ray spectra featured weak high energy tails extending above 5 keV while the majority of the X-ray signal is from an $E_e < 300$ eV population.[6] We found that the PPU model which erroneously assumed rectangular-shaped pulses does not explain the amplitude of the high-energy tail, of critical importance in warm hydrogen plasmas. In this paper, we correct spectra extracted by the standard rectangular PPU model[12] by a new PPU model, one which takes into account the shape of the pulse, trapezoidal in our system.

II. PULSE PILE-UP REDUCTION TECHNIQUES

There are numerous ways to reduce PPU and its associated artifacts. One is to reduce the solid angle viewed by the detector. This decreases the CR, decreasing PPU. It also decreases

the signal-to-noise ratio, necessitating longer integration time or creating larger uncertainty.

Another is to place a selective absorber to reduce the flux of X-rays in some regions of the spectrum. This allows the CR in the rest of the spectrum to be unchanged while the total CR is decreased. This works well, though is complicated by edges in the transmission coefficient and the difficulty in finding and fabricating a thin absorber with the correct spectral features.

Other solutions are implemented *via* signal processing: a) reducing the width of the shaped voltage pulse; b) rise-time discrimination of pulses; c) tailoring the shape of the processed pulse, *e.g.,* exponential, Gaussian, square, or triangular; and, as noted earlier, d) comparing "fast" (50 ns) channel with "slow" (1 μs) channel pulses before *vs* after pulse shaping. In the Amptek SDD system, the shape of the processed voltage pulse is trapezoidal, with equal rise and fall times, which we will refer to as t_r and a short duration "flat top", which we will refer to as t_f. For trapezoidal pulse shapes used in X-123 SDD, PPR time is rise time+flat top time.[5]

In previous plasma experiments,[6,8] the X-ray flux was low, thus long-duration measurements were needed. However, recent experiments have produced considerably higher X-ray fluxes with a more detailed spectral resolution required. Commensurably higher count rates had to be tolerated (and were appreciated).

III. PULSE PILE-UP MODEL

The photons incident on the Amptek X-123 Fast SDD generate electrons in the conduction band with a number proportional to the photon's energy. The voltage increment on the collection electrodes is measured within t_p. PPU occurs if there are multiple photons present during t_p. If the shape of the voltage is rectangular and there are multiple photons present during t_p, then the energy of the apparent photon is the sum of all the photon's energy. This creates a false count of photons with high energy and a reduction at low energy, the first most responsible for the distortion of the spectrum.

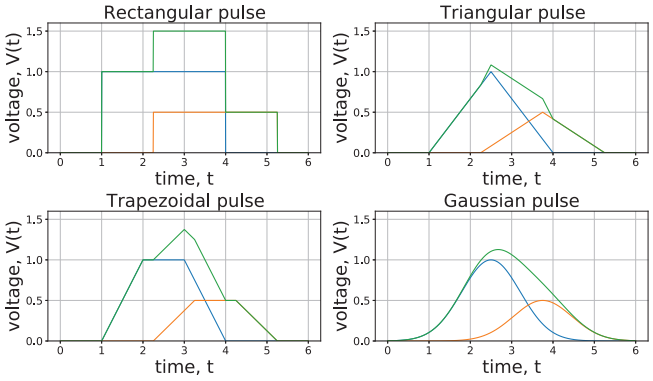

FIG. 3. Voltage *vs* time plot for two rectangular, triangular, trapezoidal, and Gaussian pulses (blue and orange) and them added together (green).

Usually, pulse-height X-ray detector systems have measures to reject PPU. An example is the aforementioned "fast channel" – "slow channel" (fc-sc) approach. Despite these measures, sometimes even the fast channel ($\sim$ 50 ns) is insufficient to resolve pile-up, such as when multiple pulses arrive within the fast channel's PPR time or when the pulses have too low an amplitude to trigger the fast channel. Under these circumstances, better mitigation techniques are required. In our experiment, the fc-sc feature was turned off, in part, because the incident UV photons are too low energy to trigger the fast channel.

In an ideal detector, where the PPR time is 0, the detector would register one X-ray photon of apparent energy E for every X-ray photon of true energy E_i. If there are X-ray photons incident upon an ideal detector at a spectral rate of $f_i(E_i)$ (units counts/eV/second), then an ideal detector measures an apparent spectral rate of $f_a(E) = f_i(E)$.

In real detectors, an X-ray photon incident at time t_i with energy E_i produces a voltage response of some specified shape $V(t-t_i,E_i)$ whose maximum value is proportional to E_i,

$$max(V(t-t_i,E_i)) = \alpha E_i \tag{1}$$

If there are multiple incident X-ray photons, then,

$$V(t) = \sum_i V(t-t_i,E_i) \tag{2}$$

$$\alpha E = max(V(t) : t_1 \le t \le t_1 + t_p) \tag{3}$$

For X-123 SDDs, the maximum is scanned within time t_p of the incident of the first photon, t_1, where $t_p = t_r + t_f$. The process is illustrated in Figure 3 with two incident photons. For every maximum of $V(t)$ within the PPR time, a non-ideal detector returns an apparent X-ray of energy E.

For a total CR μ and PPR time t_p, if two or more photons are incident within t_p, they produce a piled-up count. The probability of $n-1$ photons hitting the detector within PPR time t_p after detection of a photon follows the Poisson statistics: $P_{pois}(n-1,\mu t_p)$. The probability density of E (apparent piled-up energy bins), given that n-photon piles up is, $p_{n\gamma}(E)$. Then the total probability density of getting an apparent photon with energy E is,

$$p_a(E) = \sum_{n=1}^{\infty} P_{pois}(n-1,\mu t_p) p_{n\gamma}(E) \tag{4}$$

where the Poisson distribution[18] is $P_{pois}(n,\mu t_p) = \frac{(\mu t_p)^n}{n!} e^{-\mu t_p}$.

We develop a model for the trapezoidal voltage shape function, which includes the rectangle and the isosceles triangle as special cases. In our graphite-target experiment, the rate of incidence of X-ray photons was sufficiently low such that the effect of more than two-photon piling up is negligible. So, the model

(i) corrects the pulse shape created by photon incidence as trapezoidal

(ii) ignores the effect of pile-up from three or more photons due to the low incidence rate of X-ray.

(iii) allows no correlation between photon arrivals

IV. PROBLEMS WITH APPROXIMATING THE PULSE WITH RECTANGULAR SHAPE

We have previously modeled the process of PPU assuming rectangular pulse shapes[12] for which the piled-up spectrum can be computed using a convolution.[13] Using this method, an example of extreme PPU was simulated assuming $t_p = 10$ μs and 10^2 kcps. The results are shown in Figure 4. The true spectrum (red) is a sharp Gaussian centered around $E_\gamma = 70$ eV. The blue points are a Monte Carlo calculation showing the apparent spectrum. The yellow line is the convoluted solution that shows the apparent spectrum. The effects of PPU are clear. A long, nearly exponential tail has formed, characterized by an e-folding of $E_o \approx 50$ eV. The true X-ray spectrum can not be extracted from the piled-up data.

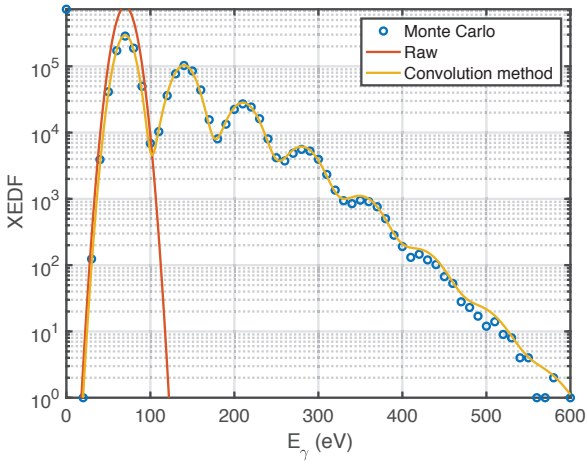

FIG. 4. Piled-up spectrum calculated from a 70 eV Gaussian distribution (red), Monte-Carlo-simulation pile-up spectrum (blue) with a rectangular pulse-shaping model and piled-up spectrum of the X-ray calculated *via* convolution (yellow).

For rectangular pulse shapes, shown in the upper left of Figure 3, the apparent energy is the sum of energies of nearly coincident X-rays. In this case, $p_{n\gamma}(E)$ takes the form of a convolution, $p_{n\gamma}(E) = \int dE'\ p(E')p_{(n-1)\gamma}(E-E')$, where $p_{1\gamma}(E) = p(E)$ is the normalized input spectrum of X-ray.

However, the rectangular pulse shape model,[12] when applied to X-ray tube data, failed to show agreement in the amplitude of the pile-up. In Figure 2, several measured and simulated X-ray energy distribution functions were compared. These X-rays were emitted from a graphite target bombarded by a 5-keV electron beam. The effect of PPU has a first or higher-order dependency on count rate as seen in Equation (4). So, the dataset with the lowest count rate (orange) was selected to represent a "clean" dataset with little pile-up. This dataset was scaled up by the ratio of count rates, to estimate the XEDF without pile-up (green). In addition, Equation (4) and convolution method were used to compute the pile-up estimate for a rectangular pulse shaping model (purple). Given that the clean lower count rate data is identical to the high count rate data set except for the pile-up tail, the predicted data (purple) should theoretically match with the higher count rate data. The rectangular model with the actual 212 ns PPR time does show a PPU tail, but an amplitude more than 2 times larger than the measured. A small "real" tail would be hidden in this large error. The rectangular model would need a PPR time of ~ 90 ns to reproduce the observed PPU tail, highlighting a shortcoming of the simple rectangular pulse-shape model in estimating the PPU.

V. DERIVATION OF PILE-UP EQUATION USING TRAPEZOIDAL MODEL

For the more accurate trapezoidal pulse shape (see Figure 3), the result is more complicated. It should be noted that for trapezoidal pulses, the second pulse's amplitude, if resolvable, is not offset by the first pulse, hence, resolvable pulses are always measured with correct amplitude. Therefore, for the case of $\mu t_p \leq 0.1$, accounting for only one and two photons is sufficient and Equation (4) can be approximated

$$p_a(E) \approx (1-\mu t_p)p(E) + \mu t_p\ p_{2\gamma}(E). \tag{5}$$

$p_{2\gamma}(E)$ needs to be expressed in terms of energy of the first and second photons, E_1, E_2, the shape of the trapezoid and PPR time t_p and $p(E)$. The shape of a trapezoidal pulse with equal rise and fall time can be expressed through three parameters, the rise time t_r, and flat top time t_f, and the height of the trapezoid corresponding to an energy E. From Figure 5,

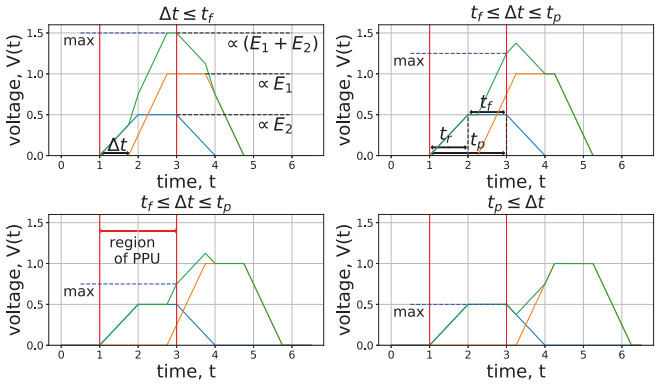

FIG. 5. Sum (shown in green) of two trapezoidal voltage pulses (blue and orange) for different values of Δt. The sum follows different pattern and formula for three different cases: $\Delta t \leq t_f$, $t_f \leq \Delta t \leq t_p$, $t_p \leq \Delta t$. For $t_p \leq \Delta t$, the pulses can be resolved and no PPU occurs.

we observe that, if the time difference between the first pulse and the second pulse is Δt, then the maximum value of the summed pulse within the region of pile up, *i.e.*, within time t_p from incidence time, is:

$$E = \begin{cases} E_1 + E_2 & \text{if, } \Delta t \leq t_f \\ E_1 + E_2(1 - \frac{\Delta t - t_f}{t_r}) & \text{if, } t_f \leq \Delta t \leq t_p \end{cases} \tag{6}$$

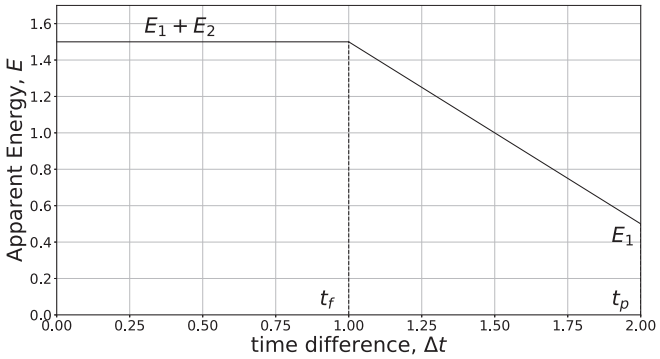

FIG. 6. Apparent energy E *vs* incidence time difference Δt where $0 \leq \Delta t \leq t_p$.

We define a shape parameter, $a \equiv \frac{t_r}{t_p}$, named the "triangularity." Triangularity $a = 0$ corresponds to a rectangular pulse while $a = 1$ corresponds to a triangular pulse.

Because Δt is uniformly distributed from 0 to t_p, the probability distribution of Δt or $p_{\Delta t}$, follows $\frac{dp_{\Delta t}}{d(\Delta t)} = \frac{1}{t_p}$. For a uniformly distributed Δt, the probability distribution of E is,

$$p_{2\gamma}(E|E_1,E_2)dE = \begin{cases} \frac{t_f}{t_p}, \text{ if } E = E_1 + E_2 \\ \frac{dp_{\Delta t}}{d(\Delta t)} \left|\frac{d(\Delta t)}{dE}\right| dE, \text{ otherwise} \end{cases} \quad (7)$$

Equation (6) can be used to differentiate the E with respect to Δt and then inverted to arrive at $|d(\Delta t)/dE| = t_r/E_2$. Using the Heaviside, $\theta(x)$, and Dirac delta, $\delta(x)$, functions, Equation (7) can be written as,

$$p_{2\gamma}(E|E_1,E_2) = \delta(E - E_1 - E_2)(1-a) + \frac{\theta(E-E_1)\theta(E_1+E_2-E)}{E_2} a. \quad (8)$$

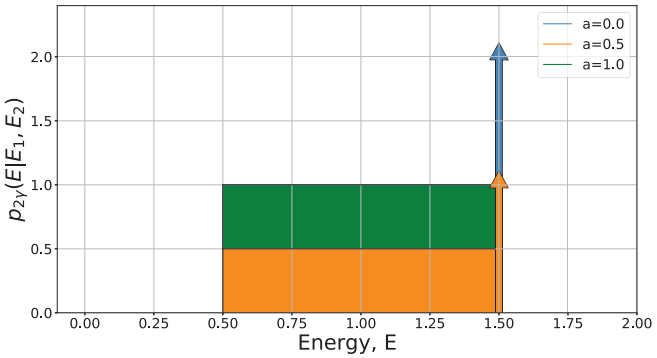

FIG. 7. Probability density function for apparent energy, $p_{2\gamma}(E|E_1,E_2)$ *vs* E for several values of the triangularity a with $E_1 = 0.5$, $E_2 = 1$. Upward arrows indicate a Dirac delta function at that value and it's height indicate the coefficient of the Dirac delta.

In Figure 7, for $a = 0$, a rectangular pulse, $p_{2\gamma}(E|E_1,E_2)$ is a Dirac delta function at the sum of the incident photon energies. For $a = 1$, a triangular pulse, the function is uniform between E_1 and E_2. For an intermediate value, a trapezoidal pulse with $a = 0.5$, both features are noticeable.

The 2-photon pile-up energy probability distribution function depends on the one photon energy spectrum as follows:

$$p_{2\gamma}(E) = \iint p_{2\gamma}(E|E_1,E_2)p(E_1)p(E_2)dE_1dE_2. \quad (9)$$

Integration of the first term $\delta(E - E_1 - E_2)p(E_1)p(E_2)$ is,

$$\begin{aligned} p_A(E) &= \iint \delta(E - E_1 - E_2)p(E_1)p(E_2)dE_1dE_2 \\ &= \int_0^E p(E - E')p(E')dE'. \end{aligned} \quad (10)$$

The integration limit of E' is from 0 to E because $p(E') = 0$ for $E' < 0$ as energy of photons can not be negative. So $p(E - E')p(E') = 0$ for $E' > E$ or $E' < 0$. In order to integrate second term, we notice that $\theta(E - E_1)\theta(E_1 + E_2 - E)$ means the integration happens in the region with $E_1 \leq E$ and $E \leq E_1 + E_2$. Meaning E_1 ranges from 0 to E and E_2 ranges (for a fixed E_1) from $E - E_1$ to infinity.

$$\begin{aligned} p_B(E) &= \iint \frac{1}{E_2} p(E_1)p(E_2)dE_1dE_2 \\ &= \int_0^E p(E') \int_{E-E'}^{\infty} \frac{p(E'')}{E''} dE''dE'. \end{aligned} \quad (11)$$

Combining results from Equations (10) and (11) and multiplying them with necessary factors gives us,

$$p_{2\gamma}(E) = p_A(E) \cdot (1-a) + p_B(E) \cdot a \quad (12)$$

These results, applied to Equation (5), produce the effect of trapezoidal voltage shape function on the energy spectrum, when accounting for 2-photon PPU. The result reduces to the rectangular model when $a = 0$. This is expected since $a = 0$ means the pulse is rectangular in which case pulses are added as in the previous model.

VI. SIMPLE PPU EXAMPLES USING TRAPEZOIDAL MODEL

Our derived formula will be applied on narrow Gaussian and truncated exponential, the latter representative of certain models.[19] The overlap probability was taken to be $\mu t_p = 0.1$. By plotting for different values of a, the effect of triangularity on the spectra were analyzed. The artificially piled-up plot of a monochromatic input spectrum (approximated by a narrow Gaussian function with FWHM=0.0526) is shown in Figure 8. There is a peak at twice the energy of the monochromatic spectrum and a constant region in between for pulses with $0 < a < 1$. There is no peak in case of triangular pulse ($a = 1$) and no constant region for rectangular pulse ($a = 0$). The constant region has a height proportional to triangularity. The constant region is also present in the Amptek DppMCA measurements

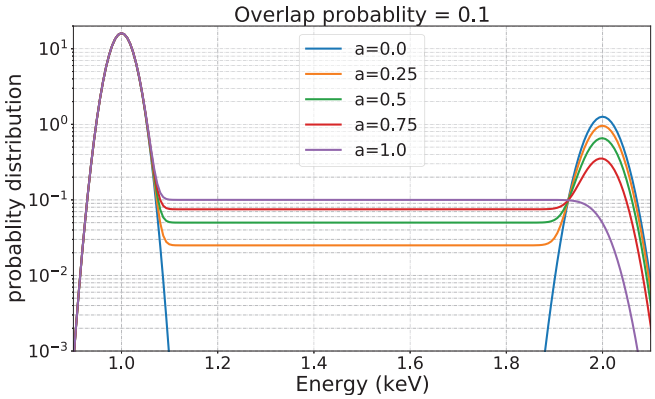

FIG. 8. Probability distribution *vs* energy plot of piled-up output of a narrow Gaussian (FWHM=0.0526) for 5 different values of triangularity.

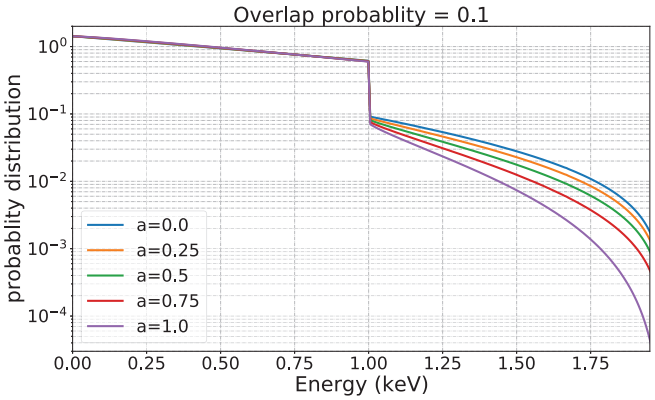

FIG. 10. PPU spectra for truncated exponential ($\propto e^{-E/E_0}$, $E_0 = 1$ keV) spectrum with cutoff at 1 keV.

for X-ray spectrum input shown in Figure 9;[20] the rectangular model ($a = 0$) is unable to explain that.

The piled-up plot of exponential function ($\propto e^{-E/E_0}$, $E_0 = 1$ keV) truncated at 1 keV is shown in Figure 10. A key thing to notice is that the pile-up tail differs by more than an order of magnitude for changing triangularity. This highlights the importance of taking pulse shape into account when modeling the PPU and illuminates why the rectangular model failed.

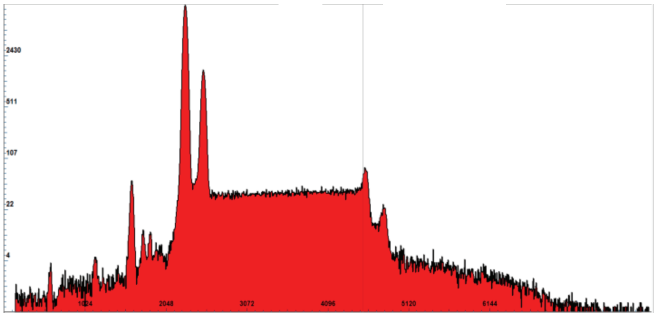

FIG. 9. 25 mm^2 Amptek (PPR disabled) DppMCA data, Zn target illuminated by X-ray tube, 30 kV. The X-ray spectrum shows similarities with piled-up Dirac delta data.[20] Horizontal axis - photon energy (eV); vertical axis - counts, log scale.

VII. EXPERIMENTAL VALIDATION OF TRAPEZOIDAL MODEL OF PULSE PILE-UP

In this section, the trapezoidal model is tested using the data collected from the graphite-target X-ray tube and compared to the rectangular pulse model. We again compare a high-count-rate (65 kcps) spectrum and predicted spectrum from scaled up low-count-rate (14 kcps) spectrum, as in Figure 2, but this time using the trapezoidal model instead of rectangular model. As before, the target voltage is 5 keV and target current was 190 nA for 14 kcps and 750 nA for 65 kcps. The pulse has a rise time and fall time of 200 ns and a flat-top time of 12 ns which means PPR time is 212 ns and triangularity, $a = 200/212 \approx 0.943$. The incidence rate of 65 kcps data is, to be exact, $\mu = 64,800$ cps. The overlap probability is $\mu t_p = 0.0137$, satisfying the two-photon approximation. The plot is shown in Figure 11 and results from Figure 2 and 11 are summarized in Table I.

The piled-up plot for 14 kcps using our trapezoid model

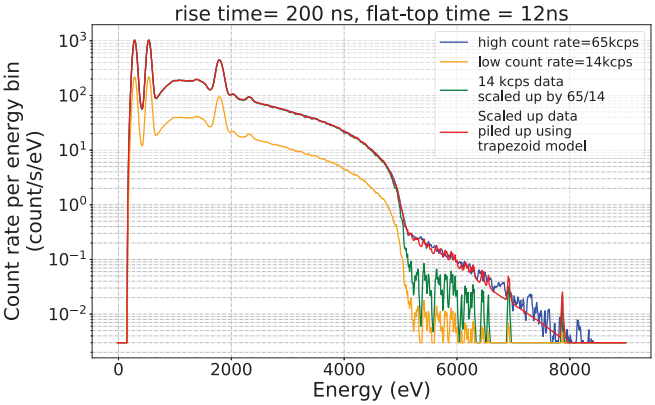

FIG. 11. 65 kcps graphite-target X-ray-tube spectrum compared with predicted spectrum derived using trapezoidal model.

shows good quantitative agreement with the natural pileup from 65 kcps. It displays an exponential shape from 5 keV to 8 keV. From the comparison between the two models in Figure 2, 11 and Table I, it is evident that the trapezoidal model accurately predicts the correct pile-up phenomenon.

VIII. SUMMARY

This paper concentrates on the continuum tail of the X-ray spectrum measured by pulse-height detector systems. In do-

Spectra \ Results	Exponential Slope	Count Rate in PPU Tail
65 kcps Spectrum	630 ± 10 eV	22.7 ± 0.5 s^{-1}
Trapezoidal Model	620 ± 10 eV	21.0 ± 0.5 s^{-1}
Rectangular Model	725 ± 10 eV	56 ± 1 s^{-1}

TABLE I. Comparison of both models with measured data

ing so, it quantifies whether tails are artifacts of PPU or real. This extends the standard use of pulse-height detectors to a new arena, one of critical importance to hydrogen plasma experiments where peaks in the X-ray spectrum are of lesser importance than the high energy tail.

It was shown that the pulse shape chosen for the output of a detector's amplifier plays an important role in the amplitude and shape of PPU tails. Because Amptek's SDD systems, the ones we use in our hydrogen plasma experiments, produce trapezoidal-shaped pulses, these were examined in most detail.

The trapezoidal model accurately predicts the PPU-modified spectrum of X-ray tube data, while the rectangular model of pulse pile-up is off by more than a half order of magnitude, showing the trapezoidal model to be accurate and that the tail in X-ray tube data is indeed an artifact of PPU when corrected for the shape of the pulse. This gives us confidence in applying it to magnetic-fusion–device spectra and for extracting the actual high energy tails which, even if a small fraction of the bulk population, can be important in determining stability, plasma resistivity, and energy transport.

The low energy part of the X-ray spectrum, below 200 eV, though far brighter than the higher energy tail and a cause of PPU, is not measured quantitatively in these experiments.

ACKNOWLEDGEMENTS

This work was supported by U.S. Department of Energy, Office of Science, Office of Fusion Energy Contract Number DE-AC02-09CH11466, ARPA-E Award No. DE-AR0001099 (Princeton Fusion Systems), and the Princeton Program in Plasma Science and Technology. We also thank Robert Redus and Benjamin M. Alessio for their comments.

DATA AVAILABILITY STATEMENT

The digital data presented in this paper are openly available on the website: http://arks.princeton.edu/ark:/88435/dsp01x920g025r. This weblink points to the collection of data for papers published by PPPL's PS&T Department. The user can then navigate to the data for this paper.

APPENDIX 1

Typical operational parameters of the Amptek X-123 Fast SDD are: Clock speed 80 MHz; 200 ns peaking time; 12 ns flat top time; 34.985 total gain (fine + coarse); 204 ns detector reset lockout; 100 ns fast channel peaking time; PUR off; RTD off; MCA channels: 1024; Peak detection mode: Normal; Slow threshold: ch 22; Fast threshold: ch 14.5; BLR mode 1 (baseline restoration); BLR up/down correction 0/3; High Voltage set: -135 V; and Temperature: 240 K.

[1] Pulse-Height Spectrometry. `https://radiologykey.com/pulse-height-spectrometry`. Accessed: December 10, 2020.

[2] Yougui Liao. *Practical Electron Microscopy and Database*. Globalsino, 2006. `https://www.globalsino.com/EM/page2532.html`.

[3] Helmuth Spieler. *Pulse Processing and Analysis*. IEEE NPSS Short Course, 2002.

[4] P. Beiersdorfer, S. von Goeler, M. Bitter, K. W. Hill, R. A. Hulse, and R. S. Walling. High-resolution bent-crystal spectrometer for the ultrasoft x-ray region. *Review of Scientific Instruments*, 60(5):895–906, 1989.

[5] X-123SDD Complete X-Ray Spectrometer with Silicon Drift Detector (SDD) – Amptek – X-Ray Detectors and Electronics. https://amptek.com/products/x-ray-detectors/sdd-x-ray-detectors-for-xrf/x-123sdd-complete-x-ray-spectrometer-with-silicon-drift-detector-sdd. Accessed: December 12, 2020.

[6] C. Swanson, P. Jandovitz, and S. A. Cohen. Using poisson-regularized inversion of bremsstrahlung emission to extract full electron energy distribution functions from x-ray pulse-height detector data. *AIP Advances*, 8(2):025222, 2018.

[7] X-ray detection by EDS. `https://myscope.training/legacy/analysis/eds/xraydetection/`. December 10, 2020.

[8] S. Cohen, C. Brunkhorst, A. Glasser, A. Landsman, and D. Welch. Rf plasma heating in the pfrc-2 device: Motivation, goals and methods. *AIP Conference Proceedings*, 1406(1):273–276, 2011.

[9] C.T. Chantler, K. Olsen, R.A. Dragoset, J. Chang, A.R. Kishore, S.A. Kotochigova, and D.S. Zucker. X-ray form factor, attenuation, and scattering tables. *NIST*, 2009.

[10] P. Jandovitz, C. Swanson, J. Matteucci, R. Oliver, J. Pearcy, and S. A. Cohen. Demonstration of fast-electron populations in a low-pressure, low-power, magnetized rf plasma source. *Physics of Plasmas*, 25(3):030702, 2018.

[11] C. Swanson and S. A. Cohen. Spontaneous multi-kev electron generation in a low-rf-power axisymmetric mirror machine. *Physics of Plasmas*, 26(6):060701, 2019.

[12] T. Rubin and T. Qian. Pulse pile-up correction for x-ray spectra measured by amptek x-123 silicon drift detector. unpublished, 2020.

[13] Dayton W. Datlowe. The role of the waveform in pulse pile-up. *Nuclear Instruments and Methods*, 145(2):365–378, 1977.

[14] Weijun Guo, Sang Hoon Lee, and Robin P. Gardner. The monte carlo approach mcput for correcting pile-up distorted pulse-height spectra. *Nuclear Instruments and Methods in Physics Research Section A: Accelerators, Spectrometers, Detectors and Associated Equipment*, 531(3):520–529, 2004.

[15] Katsuyuki Taguchi, Eric Frey, Xiaolan Wang, Jan Iwanczyk, and William Barber. An analytical model of the effects of pulse pileup on the energy spectrum recorded by energy resolved photon counting x-ray detectors. *Medical physics*, 37:3957–69, 08 2010.

[16] J. Wang, L. Chen, M. Persson, P. L. Rajbhandary, P. Kandlakunta, G. Carini, and R. Fahrig. Pulse pileup analysis for a double-sided silicon strip detector using variable pulse shapes. *IEEE Transactions on Nuclear Science*, 66(6):960–968, 2019.

[17] B. M. Alessio. Junior paper. Unpublished, Princeton University, Fall 2020.

[18] R. D. Yates and D. J. Goodman. *Probability and Stochastic Processes: AFriendly Introduction for Electrical and Computer Engineers*. Wiley, 2014.

[19] S. A. Cohen, B. Berlinger, C. Brunkhorst, A. Brooks, N. Ferraro, D. P. Lundberg, A. Roach, and A. H. Glasser. Formation of collisionless high-β

plasmas by odd-parity rotating magnetic fields. *Phys. Rev. Lett.*, 98:145002, Apr 2007.

[20] R. Redus. *Front End Electronics for Radiation Detection and Measurement*. IEEE NPSS Short Course, 2017.